MDPI

Article

Prediction of Leakage Pressure in Fractured Carbonate Reservoirs Based on PSO-LSTM Neural Network

Xuemei Xu [1,2], Xiaopeng Zhai [1,2,*] , Aoxiang Ke [1,2], Yang Lin [1,2], Xueling Zhang [1,2], Zelong Xie [1,2] and Yishan Lou [1]

[1] School of Petroleum Engineering, Yangtze University, National Engineering Research Center for Oil & Gas Drilling and Completion Technology, Wuhan 430100, China; 18327599083@163.com (X.X.); 17326075766@163.com (A.K.); 13530512930@163.com (Y.L.); zhang_xueling_123@126.com (X.Z.); 13343429174@163.com (Z.X.); louys2006@126.com (Y.L.)
[2] Hubei Key Laboratory of Oil and Gas Drilling and Production Engineering, Yangtze University, Wuhan 430100, China
[*] Correspondence: zhaixiaopeng2006@163.com; Tel.: +86-17762533797

Abstract: Shunbei Oilfield is a fractured carbonate reservoir with complex geological structures that are influenced by fault movements and prone to collapse and leak incidents. Precisely predicting leakage pressure is crucial for conducting fracturing operations in the later stages of production. However, current fracture-related leakage pressure prediction models mostly rely on statistical and mechanical methods, which require the consideration of factors such as fracture aperture and parameter selection, thereby leading to limitations in prediction efficiency and accuracy. To enhance the accuracy of reservoir leakage pressure prediction, this study leverages the advantages of artificial intelligence methods in dealing with complex nonlinear problems and proposes an optimized Long Short-Term Memory (LSTM) neural network prediction approach using the Particle Swarm Optimization (PSO) algorithm. Firstly, the Spearman correlation coefficient is used to evaluate the correlation between nine parameter features and leakage pressure. Subsequently, an LSTM network framework is constructed, and the PSO algorithm is applied to optimize its hyper-parameters, establishing an optimal model for leakage pressure prediction. Finally, the model's performance is evaluated using the Coefficient of Determination (R^2), Root Mean Squared Error ($RMSE$), and Mean Absolute Percentage Error ($MAPE$). The evaluation results demonstrate that the PSO-optimized LSTM model achieved an R^2 of 0.828, $RMSE$ of 0.049, and $MAPE$ of 3.2, all of which outperformed the original model. The optimized LSTM model showed an average accuracy approximately 12.8% higher than that of the single LSTM model, indicating its higher prediction accuracy. The verification results from multiple development wells in this block further confirmed that the deep learning model established in this study surpassed traditional methods in prediction accuracy. Consequently, this approach is beneficial for drilling engineers and decision-makers to plan drilling operations more effectively and achieve accurate risk avoidance during the drilling process.

Keywords: fracture leakage; deep learning; Long Short-Term Memory (LSTM) neural network; Particle Swarm Optimization (PSO) algorithm

1. Introduction

Wellbore leakage refers to a complex downhole situation that occurs during drilling, cementing, testing, and other operations, in which the working fluid leaks into the formation due to pressure differentials. Calculating the leakage pressure accurately is challenging due to factors such as subsurface geological complexity, fluid behavior complexity, and uncertainty in engineering parameters. When wellbore leakage occurs, it can lead to wasted drilling time, the loss of drilling fluid and plugging materials, and even damage to the reservoir, which impacts subsequent oil recovery operations. Therefore, determining the leakage pressure of the formation is critical for improving the success rate of leak prevention

and plugging, and it provides crucial guidance in deciding whether reservoir fracturing operations should be conducted.

The traditional calculation methods commonly used can be classified into empirical formula calculations and statistical calculation models [1–4]. The mechanical model primarily analyzes from a mechanical perspective. When the mud column pressure increases during drilling, the radial stress around the wellbore also increases, while the tangential stress decreases. If the combined radial and tangential stresses cause shear failure in the formation at the location of the maximum horizontal earth stress, fractures are assumed to appear around the formation, resulting in formation leakage. At this point, the mud column pressure is considered as the leakage pressure. However, the results obtained from this mechanical model tend to be larger than the actual values. This discrepancy arises mainly because the mechanical model is derived under non-leakage conditions. It relies on empirical coefficients and existing experimental data, has limited applicability, and may be inaccurate for complex well leakage situations, lacking in details and precision. Breckels [5] proposed a method for determining the minimum horizontal principal stress, known as the minimum envelopment method, to estimate formation leakage pressure during drilling operations. This method assumes that formation leakage occurs due to wellbore fracturing, and that the leakage pressure is closely related to the minimum horizontal principal stress. It has been applied in engineering with reasonable accuracy. However, this method simplifies the assumptions regarding geological and fluid behavior, failing to accurately reflect the complexity and diversity of actual wellbore leakage behavior. Statistical-based models for calculating leakage pressure are derived from the analysis of a large amount of field data on wellbore leakage. Factors such as drilling fluid density, viscosity, and characteristics of the leakage pathway in the formation influence wellbore fluid loss. The statistical analysis of leakage rates through porous formations is used to establish a relationship model between pressure differential and leakage rate. This model, compared to mechanically based leakage pressure models, is more practical and widely applicable as it better aligns with reality. However, the parameters in this model are influenced by multiple factors and cannot be determined with certainty. To achieve more accurate predictions of leakage pressure, recent studies have focused on developing calculation models specifically tailored for fissured and permeable formations [6]. Zhai [7] established a dynamic model for leakage pressure based on parameters such as time, leakage rate, and crack width, controlling variations in induced fractures to manage leakage pressure. Researchers such as Ozdemirtas, Majidi, and Shahri [8–15] have investigated drilling fluid leakage models for fissured formations for different dimensions, flow patterns, and crack smoothness. Each model considers different perspectives and has a different applicability and range of application. For complex geological structures and fluid behavior, more sophisticated models and calculation methods may be required, posing computational challenges.

With the further development of machine learning in the oil and gas industry, data-driven methods are revolutionizing the field. Deep learning, as a prominent branch of machine learning, offers unique advantages in data processing, and researchers have conducted studies in various areas of the oil and gas industry [16–30]. Panja [16] used three different machine learning methods to predict hydrocarbon production in hydraulic fracturing wells, and the results showed that the prediction performance of the least squares support vector machine was the best. Ahmed [17] established a real-time prediction model for vertically complex lithological stacking density based on drilling parameters, which can be applied to the calculation of stacking density for various lithologies. Agin [18] employed an adaptive neuro-fuzzy inference system (ANFIS), data mining, and experimental design methods to predict formation leakage. In their comparisons, they found that the results obtained from the adaptive neuro-fuzzy inference system were accurate. Abdulmalek [22] used support vector machines based on well logging data and surface drilling parameters to establish models for predicting formation pore pressure and fracture pressure. These models can estimate pore pressure without the need for pressure trends and predict fracture pressure solely based on easily obtainable real-time surface drilling parameters. Wang [25]

proposed a deep learning method for porosity prediction based on a deep bidirectional recurrent neural network. The results showed that compared to the fully connected deep neural network method, this approach not only effectively addressed the issue of spatial scale in porosity prediction but also compensated for the deficiency of traditional deep networks in providing contextual information. Consequently, it improved the accuracy and stability of porosity prediction. Yang [26] used shale gas well production data to establish a database for training recurrent neural network models. The LSTM model showed good scientific accuracy and predictive performance in both short-term and long-term forecasts. It achieved accurate production prediction for neighboring wells and demonstrated high conformity with actual shale gas production. Luo [27] applied both backpropagation neural network (BP) and LSTM deep learning networks to intelligently predict formation porosity pressure. The test results indicated that the LSTM neural network model had superior predictive performance. Due to the complexity of geological structures, most geological features exhibit temporal characteristics, and the prediction of leakage pressure demands high accuracy and adaptability. PENG [28] applied LSTM-based models for energy consumption prediction and compared them with several popular models. The LSTM models consistently exhibited higher predictive accuracy when compared to other current models. Considering the above, we choose the Long Short-Term Memory (LSTM) network. LSTM is an improved and enhanced version of conventional Recurrent Neural Networks (RNN). It addresses issues such as the vanishing gradient problem in conventional RNNs through fine-tuning the design of the network's recurrent body. The most significant difference in a recurrent neural network lies in the interconnectedness of its hidden layers, where each hidden unit is not only related to others but is also influenced by the temporal input received by that hidden unit in the past. This characteristic is especially beneficial for handling data that are time dependent. By using this approach, the predicted leakage pressure takes into account the intrinsic relationships between different features and their changing trends with depth. As a result, it accurately calculates the leakage pressure in different formations.

However, traditional network prediction models often involve complex computations and require the manual tuning of hyper-parameter values to achieve optimal training results, consuming a considerable amount of time. Considering the use of heuristic optimization algorithms to handle hyper-parameters, commonly used heuristic optimization algorithms include Particle Swarm Optimization (PSO), Genetic Algorithm (GA), Differential Evolution (DE), etc. Ehsan [31] utilized four machine learning (ML) methods and two traditional Rate of Penetration (ROP) models to predict drilling speed. They applied heuristic optimization algorithms and the backpropagation algorithm for ML model prediction, and the results indicated that combining machine learning with heuristic optimization algorithms achieved the highest prediction accuracy. Wang [32] introduced a novel hybrid shear wave velocity prediction model that combines the Particle Swarm Optimization (PSO) algorithm with optimized Long Short-Term Memory (LSTM) recurrent neural networks. This model incorporates adaptive learning strategies and demonstrates superior prediction accuracy and robustness compared to traditional methods. One of the key advantages of the PSO algorithm is its ability to utilize parallel computing resources effectively, which accelerates the optimization process and makes it suitable for handling large-scale optimization problems. In particular, when dealing with a high number of optimization parameters, PSO can achieve rapid and precise results. In light of these advantages, this paper proposes an enhanced Long Short-Term Memory (LSTM) model for predicting leakage pressure using the PSO algorithm. The Particle Swarm Optimization (PSO) algorithm is well-known for its strong global optimization capabilities and fast convergence speed. By employing PSO to optimize the hyper-parameters of the LSTM model, the prediction accuracy of the model can be significantly improved. Moreover, this optimization approach eliminates the need for laborious and specialized model tuning procedures, making it more user-friendly for field personnel.

2. Methods and Principles

2.1. Principles of LSTM Recurrent Neural Networks

LSTM was originally proposed by Hochreiter [33], and in 2000, Schmidhuber et al. improved the LSTM network by introducing the method of forget gates, which is suitable for continuous prediction. Subsequently, Grave further improved and extended LSTM in his book [34–41]. The predecessor of the LSTM neural network is the Recurrent Neural Network (RNN), which learns sequential patterns through internal loops. RNN has multiple recurrent loops that allow information to be continuously passed along. Hochreiter introduced memory cells and gates, which enabled the long-term storage of information while forgetting unnecessary information. In the LSTM network, a memory cell is used instead of a neuron. An LSTM cell consists of one memory cell (c_t) and three gate structures, including an input gate (i_t), a forget gate (f_t), and an output gate (o_t). At time step t, x_t represents the input data, and h_t represents the hidden state. The equations for LSTM operations are shown in Equations (1)–(6):

$$f_t = \sigma(U_f x_t + W_f h_{t-1} + b_f) \tag{1}$$

$$i_t = \sigma(U_i x_t + W_i h_{t-1} + b_i) \tag{2}$$

$$u_t = \tanh(U_u x_t + W_u h_{t-1} + b_u) \tag{3}$$

$$c_t = f_t * c_{t-1} + i_t * u_t \tag{4}$$

$$o_t = \sigma(U_o x_t + W_o h_{t-1} + b_o) \tag{5}$$

$$h_t = o_t * \tan h(c_t) \tag{6}$$

In the equations, U and W represent matrix weights, b represents the bias term, the symbol '×' denotes vector outer product, and the symbol '+' represents addition. σ denotes the sigmoid activation function, which outputs values in the range [0, 1]. In this range, 0 indicates "completely forgetting all information", and 1 indicates "completely retaining all information". The expression for the sigmoid function is:

$$sigmoid(x) = \frac{1}{1 + e^{-x}} \tag{7}$$

The forget gate calculates the weighted sum of x_t and h_{t-1}, and applies the sigmoid function to obtain f_t ($f_t \in (0, 1)$), as shown in Equation (1). f_t represents the weight of the information to be forgotten in the previous memory cell (C_t). In other words, the forget gate controls the amount of information retained in the previous memory cell, as shown in Equation (4). The input gate determines how much new information should be received into the memory cell (C_t), and C_t represents the storage weight of the memory cell. The original information and the new information are controlled by the forget gate and the input gate, respectively, to obtain the current memory cell (C_t). Finally, the output gate, as shown in Equation (5), filters the memory cell (C_t). The updated memory cell obtains the current hidden state value through Equation (6). Finally, backpropagation is performed to obtain the LSTM model composed of these storage blocks, as shown in Figure 1.
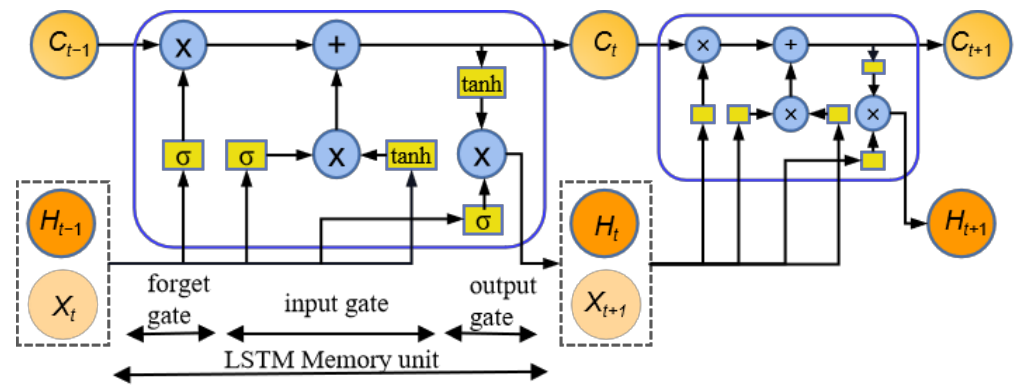
Figure 1. LSTM network structure.

2.2. PSO Algorithm

Particle Swarm Optimization (PSO) is a heuristic optimization algorithm proposed by Kennedy and Eberhart [42]. This algorithm mimics the foraging process of bird flocks to search for the optimal solution [43–47]. In the PSO process, particles update their positions and velocities based on individual best and global best. The particle's position is denoted as p_i^k; the individual best represents the position of a particle with the lowest error along its movement trajectory, denoted as p_i^*; and the global best represents the position of a particle with the lowest error among all particles along their movement trajectories, denoted as g^*. The particles update their velocities and positions iteratively:

$$v_i^{k+1} = \omega v_i^k + c_1 r_1 (p_i^* - x_i^k) + c_2 r_2 (g^* - x_i^k) \tag{8}$$

$$p_i^{k+1} = p_i^k + v_i^{k+1} \tag{9}$$

In the equation, v_i^k and x_i^k represent the velocity and position of the *i*-th particle in the *k*-th iteration; c_1 and c_2 are two constants representing individual cognition and swarm cognition, respectively; r_1 and r_2 are two random numbers within the range [0, 1]. ω represents the inertia weight, which denotes the degree of influence of the previous iteration's velocity. Linear decrement is employed to adjust the inertia weight, ensuring that it is relatively large during the early stages of global exploration and gradually decreases with an increase in iteration count. This approach promotes a balance between global exploration and local convergence.

The particle positions are iteratively updated until the minimum error criterion is reached or the maximum iteration limit for particle updates is reached.

2.3. Model Building Based on PSO-Optimized LSTM

The traditional LSTM model is a single intelligent prediction technique in which the parameter values of the model are randomly set, leading to long training time and low prediction accuracy. The Particle Swarm Optimization (PSO) algorithm has strong self-learning ability and global search capability for optimal parameters. It has been widely used to solve complex optimization problems in various fields with significant optimization effects. By using the PSO algorithm to optimize the hyper-parameters of the Long Short-Term Memory (LSTM) neural network algorithm model, the computational burden of parameter optimization in traditional models can be greatly reduced. In machine learning models, it is common to select hyper-parameters such as the number of hidden layers (Numhiddenunits), learning rate (Initiallearnrate), number of iterations (Max epoch), minimum training batch size (Batch size), and activation function. In the context of this paper, which focuses on solving a data regression problem, we select the initial learning rate, number of iterations, minimum training batch size, and number of hidden layer neurons as the hyper-parameters to be optimized.

The specific process of model construction and computation is presented in a flowchart as shown in Figure 2. Firstly, the data processing module performs data cleaning and normalization on the known well logging data. The purpose is to eliminate invalid data and remove the influence of dimensional differences among parameters. Then, the data are divided into training data and testing data. The LSTM prediction model is built, and it is trained using the combination of LSTM model and the hyper-parameters obtained through PSO optimization. Finally, the optimal parameters are saved, and the resulting model is considered as the predictive model in this study.
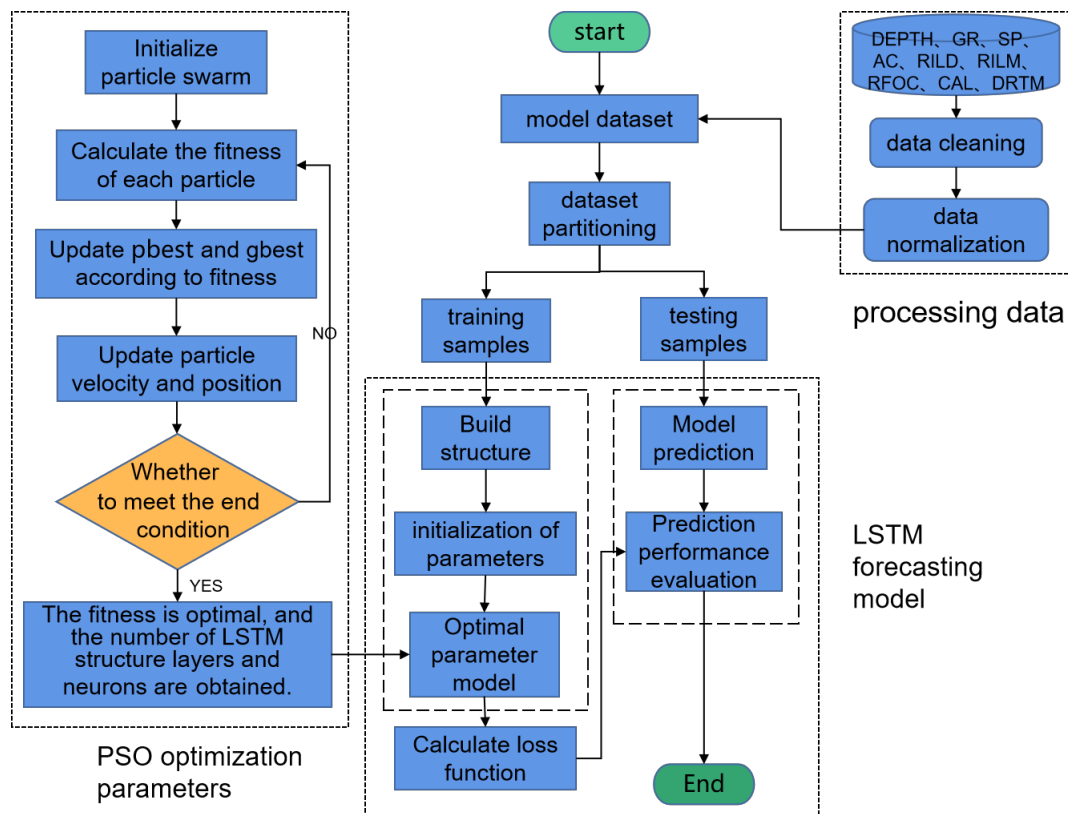
Figure 2. Block diagram of the PSO-LSTM network implementation process.

3. Experiment and Result Analysis

3.1. Correlation Analysis

The training dataset described in this paper consists of 9 input features and 1 output feature. Using too many input features in the development of neural network models will slow down the model training process and may lead to overfitting of the dataset. Therefore, it is necessary to perform feature selection to remove redundant and irrelevant input features from the dataset. This will improve the computational efficiency of the model and reduce overfitting. If all well logging curves are directly used to build a linear or nonlinear model between well logging curves and lost circulation pressure parameters, it would not only increase the complexity of the model but also result in the loss of useful information or the introduction of redundant information, leading to a lack of accuracy in the model. Therefore, selecting the appropriate well logging curves for constructing the sample data is of great importance. Choosing well logging curves with a high correlation to reservoir parameters and lost circulation pressure as input features will effectively improve the performance of the model.

In this study, Spearman's rank correlation coefficient and Pearson's correlation coefficient are used to quantitatively measure the relationship between well logging data and lost circulation pressure. The relationship is depicted in Figure 3. In the calculation of the

correlation between well logging curves and lost circulation pressure, certain well logging curves, such as deep resistivity (RILD), shallow resistivity (RFOC), medium resistivity (RILM), acoustic transit time (AC), spontaneous potential (SP), well depth (Depth), natural gamma (GR), and drilling time (DRTM), exhibit high correlation coefficients with lost circulation pressure. This indicates a strong correlation between these well logging curves and lost circulation pressure, and these well logging curve data also have an impact on lost circulation pressure in practice, making them suitable as feature inputs for predicting lost circulation pressure. Figure 4 displays a heat map of the correlation coefficients determined by Pearson's input parameter standards and the network model. The heat map is used to identify the collinearity among input parameters.
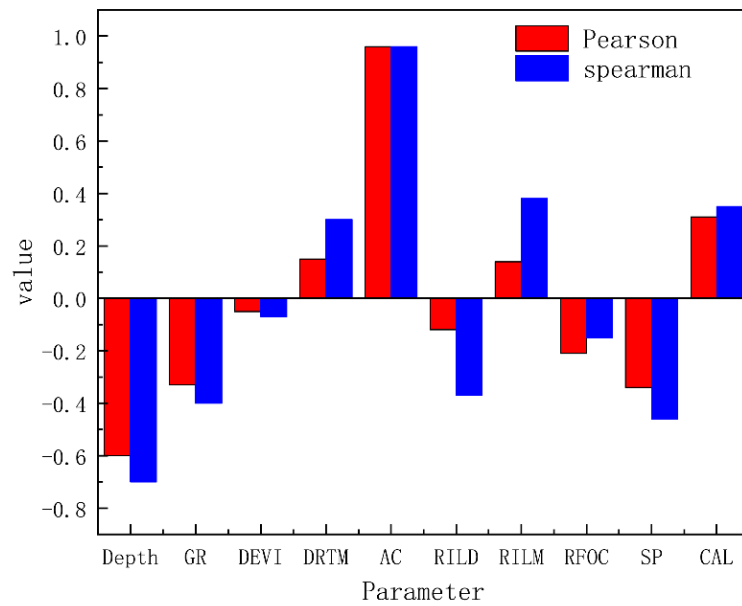

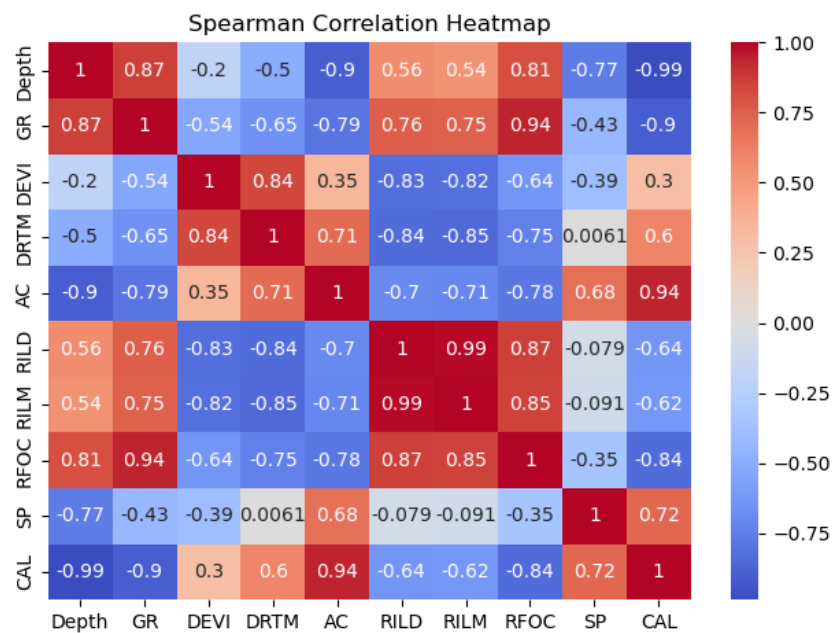**Figure 3.** Correlation analysis with leakage pressure.

Figure 4. Spearman correlation coefficient heat plot of the dataset.

3.2. Data Normalization

The partial well log curve data of a well in a certain block discussed in this paper are shown in Table 1. The features in the training dataset have different units, resulting in different scales. If there is a significant difference in scales, it can affect the results of data analysis and learning. To eliminate the influence of different scales among parameters, it is necessary to perform data standardization, which enhances the comparability among parameters. The standardized features will follow a standard normal distribution, expressed by the equation:

$$z_{ij} = \frac{x_{ij} - \mu_i}{\delta_i} \tag{10}$$

Table 1. Logging curve data table.

S/N	Production Parameters	Min	Max	Average	STD
1	SP	76.239	76.239	62.99	4.14
2	GR	50.61	258.12	79.90	14.52
3	RILD	0.179	2.20	0.62	0.33
4	RILM	0.21	1.53	0.62	0.27
5	RFOC	0.27	2.10	0.71	0.26
6	AC	63.31	107.54	82.77	7.16
7	CAL	0.02	0.83	0.36	0.17
8	DEVI	1	44	1.45	2.26
9	DRTM	1.02	1.99	1.36	0.17

In the equation, μ and δ represent the mean and standard deviation of each parameter, i represents different feature parameters, and j represents the sample of each parameter. The quantized features will be distributed in the range $[-1, 1]$.

First, the training data are standardized and the standardization parameters are retained. Then, these standardization parameters are used to standardize the test data. The separate standardization of training and test data ensures their independence. Using the same standardization parameters as the training data ensures that the test data are standardized within the distribution range of the training data, making it compatible with the parameters of the network model for training and prediction. After achieving the desired performance of the network model, when handling unlabeled data in practical applications (data without leakage pressure), the data only need to be processed using the same standardization process as the test data. This allows the trained network model to predict leakage pressure for unknown data.

4. Case Analysis

The data used in this study is from Block A of the Shunbei Oilfield. The oilfield is a complex Ordovician carbonate fracture-cave reservoir with a burial depth exceeding 7000 m. The area is characterized by complex geological structures and is influenced by fault movements, making it prone to fissure-type leakage. Some well sections have experienced severe and continuous leakage accidents. Through the statistical analysis of well logging data, this study selects the geological engineering parameters necessary for interpreting formation conditions as feature values to create the dataset. These parameters include natural gamma ray, natural potential, deep induction resistivity, medium induction resistivity, sonic transit time, drilling time, and well depth. These nine feature parameters are used to predict formation leakage pressure, with the actual leakage measurements in the field serving as the basis. Before inputting the data into the neural network for training, the should be divided into a training set and a test set. Based on the available well logging data, there are a total of 26 wells that can be used for experimentation. The logging curve for one well is shown in Figure 5; each well has approximately 15,000 samples of leakage pressure data. Of the consecutive samples, 20% are selected as the test dataset, and the remaining samples are used as the training dataset.
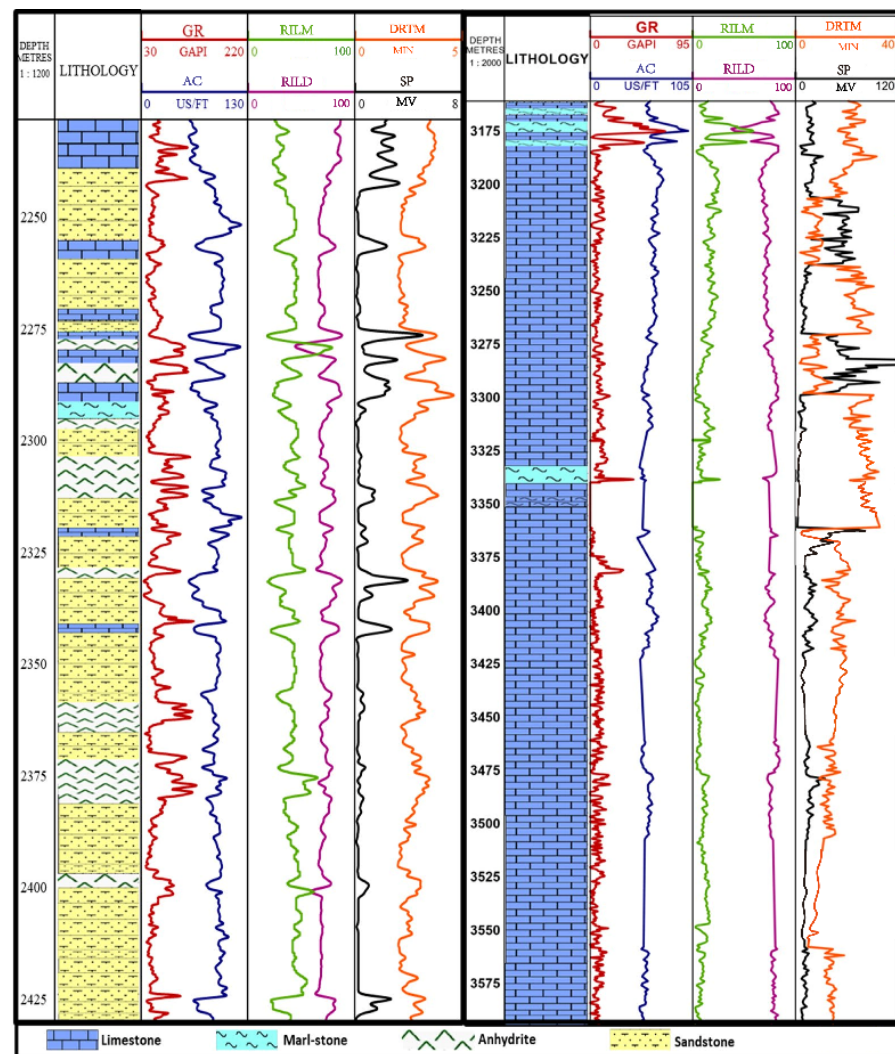
**Figure 5.** Well H logging curve of Block A of Shunbei Oilfield.

Using forward propagation, the training data are input into the network to compute the output values of the LSTM units. Then, through two fully connected layers, feature extraction is performed layer by layer until reaching the output layer, obtaining the "predicted estimate" for the current sample data. The error terms of each neuron are then calculated in reverse. The backpropagation of the LSTM recurrent neural network error terms involves two directions: one is the backward propagation along the time sequence, starting from the current time step ω and computing the error term for each time step; the other is the propagation of the error term to the previous layer. The mean squared error (MSE) is used as the loss function, and the Adam algorithm with gradient descent is employed to optimize the weights in the model based on the corresponding error terms. The gradients of each weight are computed to adjust the model parameters, moving the predicted results closer to the optimization objective. Early stopping is used to prevent overfitting. In the LSTM model, the initial values of the parameters are typically set based on experience, and then continuously adjusted through experimentation to obtain suitable parameter values. In this study, the parameters lr, u, and batch_size in the LSTM model are optimized within the ranges shown in Table 2. The PSO algorithm mainly includes parameters such as the number of particles (pop), dimensionality of the particle swarm (dim), maximum number of iterations (max_iter), inertia factor (ω), acceleration constants (c_1 and c_2). Based on experience, pop is initialized as 20, and dim represents the number of attribute features input into PSO; thus, dim is set to 7. Through iterative optimization, suitable parameter

values and hyper-parameter settings are obtained as shown in Table 2, resulting in an LSTM Recurrent Neural Network prediction model that meets the error requirements.

Table 2. Variable values before and after LSTM network layer function optimization.

| Function	Parameter	Initial Value	Optimization Range	Optimized Value
Training Options	Max Epochs	40	[40, 200]	100
	Learn Rate	0.0001	[0.0001, 0.1]	0.001
	Min Batch Size	64	[64, 640, 32]	64
	Input Size	7	-	7
LSTM Layer	Hidden layer	10	[10, 100]	20
	Bias	32	-	32
	Output Size	1	-	1
Fully Connected LayerPSO	Pop	20	-	
	Dim	7	-	

During the training process of a neural network, a loss function is typically used to measure the model's ability to fit the training data. The neural network algorithm adjusts the model parameters (i.e., the weights of the network) through multiple training iterations. The decreasing trend in the loss function is used to determine whether the algorithm has achieved an ideal deep neural network model. Figure 6 shows the loss function plot before and after optimizing the hyper-parameters using PSO. From the loss function plot, it can be observed that the PSO-LSTM model exhibits good performance, reducing the loss function value by approximately 8% and improving the prediction accuracy.
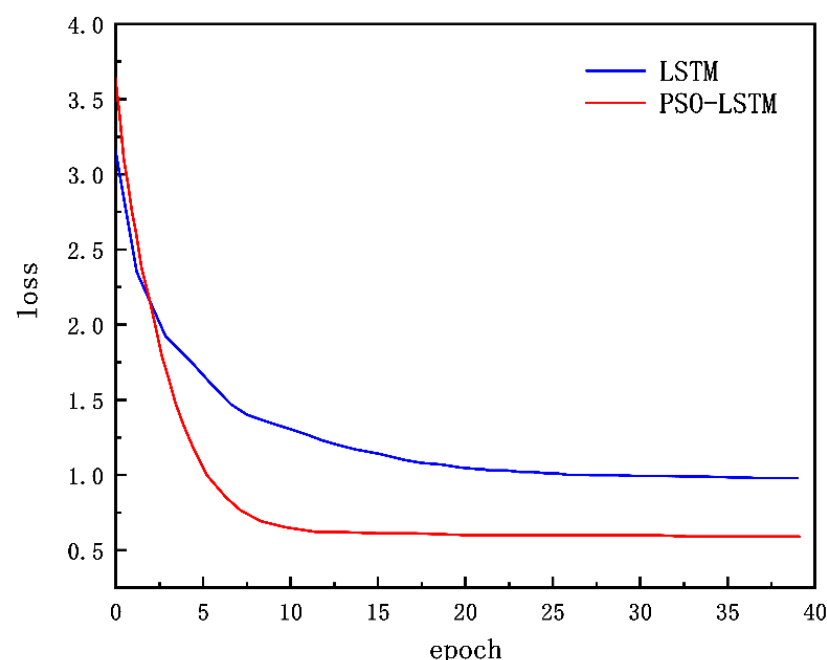
Figure 6. Comparison of loss values.

After multiple rounds of training on the data from 20 wells, a set of parameters and hyper-parameters with the best performance was obtained. These parameters were then used to validate wells 1–10. Firstly, the LSTM model's prediction results on the test set and training set are shown in Figure 7a. It can be observed that there is a relatively good relationship between the predicted values and the true values in both the training and test sets. At this point, the error value for the training set is 1.02%, while the error value for the test set reaches 1.52%. This can be attributed to two factors: First, although the data volume is relatively large, the small intervals between the data points result in similar data features,

limiting the network's ability to extract more distinctive features and leading to increased prediction errors. Second, it indicates that the traditional LSTM has certain limitations in prediction and cannot be manually adjusted to the optimal level. Next, the training and test results obtained using the model optimized with PSO for hyper-parameters are shown in Figure 7b. At this stage, the accuracy is improved by approximately 12.8% compared to the single LSTM model.

(a)

(b)
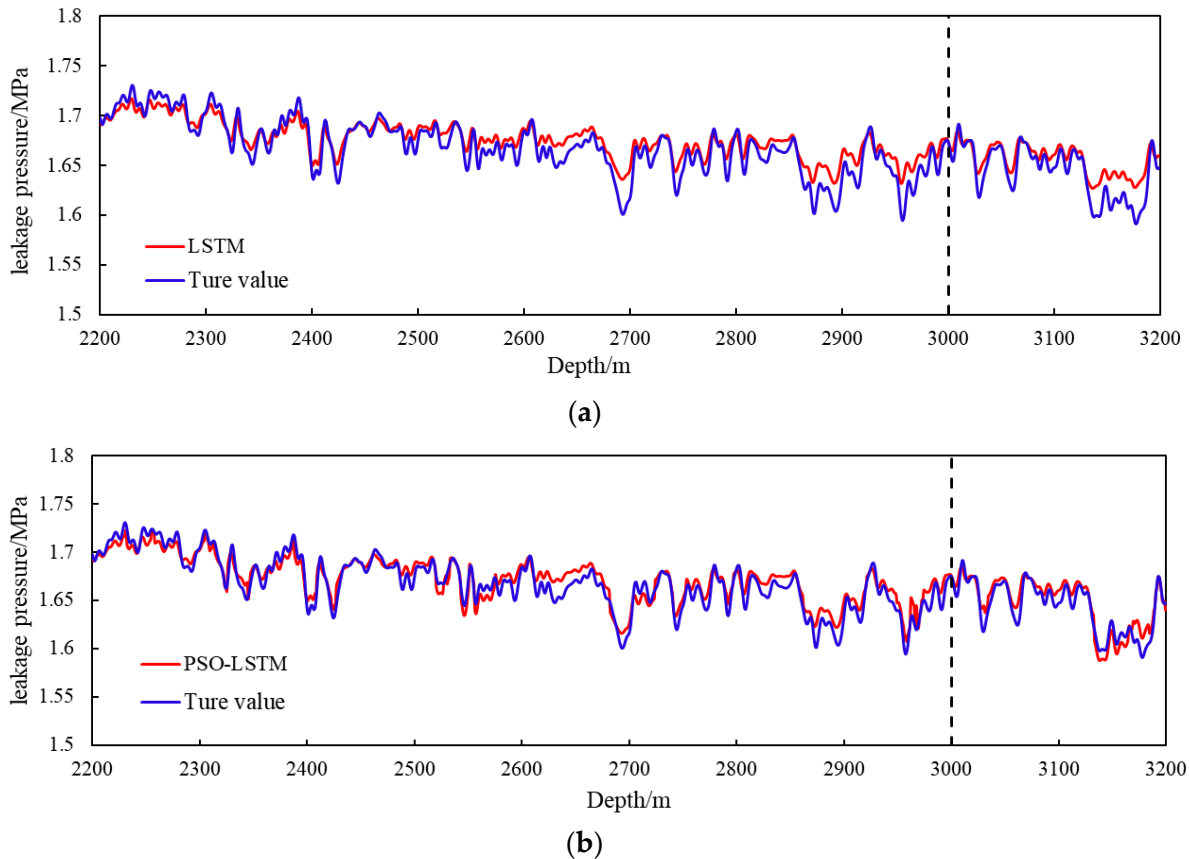
Figure 7. Comparison of model prediction results before and after Particle Swarm Optimization: (**a**) model prediction results before PSO optimization; (**b**) model prediction results after PSO optimization.

For a development well in the same block with a known leakage measurement point, the leakage pressure is predicted using the aforementioned model. The predicted results are compared with those obtained from statistical models, empirical calculation models, and the actual on-site leakage measurement point, as shown in Figure 8. The calculation formulas for the statistical models and empirical models are as follows:

$$Q = K \cdot \Delta p^n \tag{11}$$

$$P_l = \sigma_h \tag{12}$$

In the equations: Q represents the leak rate, K is the leak intensity coefficient, Δp is the pressure difference, n is a coefficient describing the state of drilling fluid leakage, P_l represents the leakage pressure, and σ_h is the minimum horizontal earth stress.

The results obtained from the model proposed in this paper were found to be much closer to the actual measurement points, providing better on-site guidance. The well section from 5770 m to 6221 m experienced multiple occurrences of well leakage, and continuous leakage was observed. For this well section, measures such as leak plugging and leak prevention should be taken, and fracturing operations should not be conducted in the sections with continuous leakage.
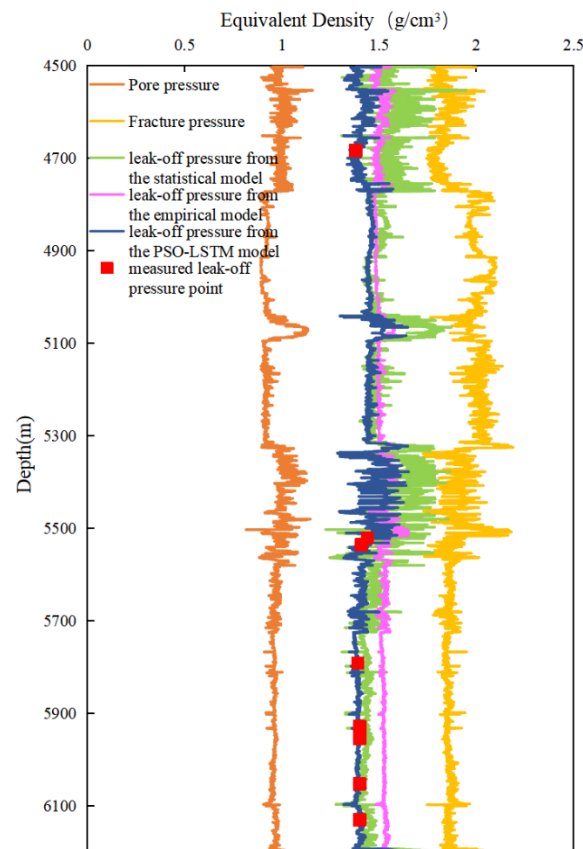
Figure 8. A comparison chart of leakage pressure and measured point of leakage point calculated by three models of development well.

Model Evaluation

The leakage pressure prediction model constructed in this paper belongs to a regression forecasting model, and the accuracy of the model's predictions is the fundamental basis for evaluating its performance. In practical research, there are many different evaluation metrics to assess the model's performance, but each metric has its own focus. Therefore, when selecting evaluation metrics for the leakage pressure prediction model, it is essential to consider both the characteristics of the model itself and the implications represented by each evaluation metric. The performance evaluation metrics of this model in this study include Root Mean Squared Error ($RMSE$), Coefficient of Determination (R^2), and Mean Absolute Percentage Error ($MAPE$). The calculation formulas for these metrics are as follows:

$$RMSE = \sqrt{\frac{1}{m}\sum_{i=1}^{m}(y_i - \hat{y}_i)^2} \tag{13}$$

$$R^2 = 1 - \frac{RSS}{TSS} \tag{14}$$

$$MAPE = \frac{1}{m}\sum\left(\left|\frac{(y_i - \hat{y}_i)}{y}\right|\right) \cdot 100 \tag{15}$$

In the equations, y_i and $\hat{y}_i$ represent the actual and predicted values of the leak pressure, RSS represents the sum of squared residuals, and TSS is the total sum of squares. Through the analysis and comparison of various error metrics of the network models, it was observed that the LSTM model based on PSO optimization achieved better prediction accuracy compared to the original model. The correlation between predicted values and actual values is shown in Figure 9. The R^2 error and Root Mean Squared Error ($RMSE$) for training and testing before and after PSO optimization are shown in Table 3. After

optimization, the R^2 error increased by 4.7%, the *RMSE* decreased by 9.4%, and the *MAPE* decreased by 43.85%.
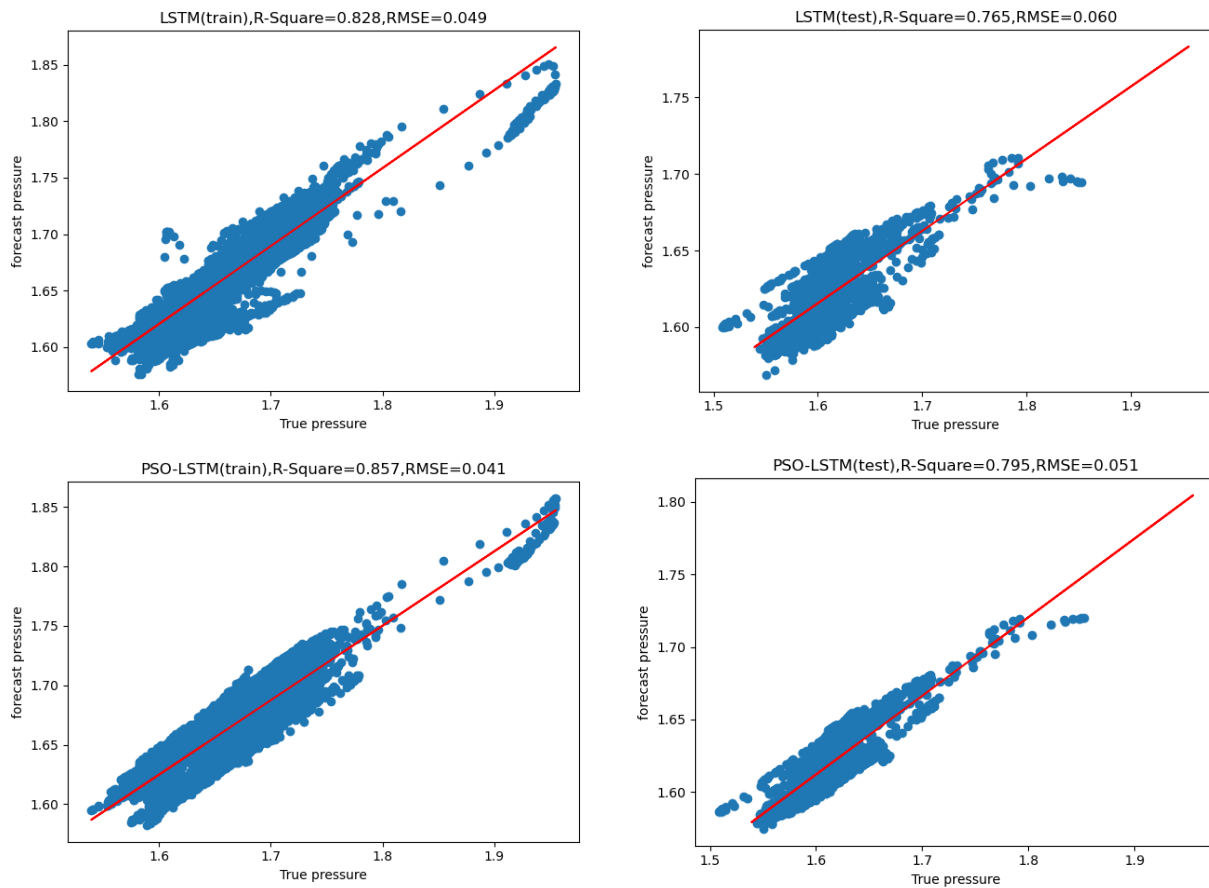
Figure 9. Correlation between the predicted values and the true values of the training and test sets.

Table 3. The statistical evaluation metrics results for the model are as follows.

Method	Train			Test		
	R^2	*RMSE*	*MAPE*	R^2	*RMSE*	*MAPE*
LSTM	0.828	0.049	5.7	0.765	0.060	8.9
PSO-LSTM	0.857	0.041	3.2	0.795	0.051	7.5

5. Conclusions

This paper introduces a novel approach that utilizes the Particle Swarm Optimization (PSO) algorithm to automatically optimize the hyper-parameters of a Long Short-Term Memory (LSTM) neural network model. The model is trained using multi-block oil and gas data from the Shunbei region. Comparative analysis reveals that our proposed PSO-optimized LSTM model overcomes the limitations of traditional methods, offering advantages such as faster convergence, shorter training time, and higher training efficiency compared to a single model. The evaluation of the model yields impressive results, with an R^2 value of 0.828, *RMSE* of 0.055, and *MAPE* of 3.2, demonstrating improved accuracy and effectiveness compared to the non-optimized model.

Based on the predicted results from a development well with a known leakage measurement point, we observe that the PSO-LSTM model provides results that closely match the actual leakage measurement point. Its accuracy significantly surpasses that of traditional empirical and statistical calculation models, offering leakage pressure predictions that align

better with real on-site conditions. The accurate prediction of leakage pressure serves as a valuable theoretical basis for post-production reservoir depletion fracturing operations.

The standalone standard LSTM algorithm's lower efficiency, due to randomly chosen hyper-parameters, is addressed effectively through combination with the PSO optimization algorithm (PSO-LSTM). By selecting optimal hyper-parameters for the LSTM model, especially through rigorous feature selection, the model's performance is significantly improved. This approach holds potential for widespread application in predicting leakage pressure in similar lithological formations. Future research aims to test this model with datasets from different lithologies and further optimize the method for selecting well logging features in various geological contexts.

Author Contributions: Conceptualization, X.X. and X.Z. (Xiaopeng Zhai); methodology, X.X.; software, A.K.; validation, Y.L. (Yang Lin); formal analysis, X.Z. (Xueling Zhang); investigation, Z.X.; resources, Y.L. (Yishan Lou); data curation, Z.X.; writing—original draft preparation, X.X.; writing—review and editing, Y.L. (Yang Lin); visualization, X.Z. (Xiaopeng Zhai); supervision, A.K.; project administration, X.Z. (Xueling Zhang); funding acquisition, Y.L. (Yishan Lou). All authors have read and agreed to the published version of the manuscript.

Data Availability Statement: The specific data involved in this paper is confidential and cannot be disclosed without authorization.

Conflicts of Interest: The authors declare no conflict of interest.

References

1. Jin, Y.; Chen, M.; Liu, X.M.; Li, Z.J. Statistic analysis of leakage pressure of Ordovician carbonate for mation in middle Ta-rim Basin. *Oil Drill. Prod. Technol.* **2007**, *29*, 82–84.
2. Zhu, L.; Zhang, C.Y.; Lou, Y.S.; Sun, W.H.; Li, Z.H.; Wu, H.M. Comparative analysis between the mechanics-bused and statistics-based calculation models for leakage pressure. *Nat. Gas. Ind.* **2008**, *28*, 60–61.
3. Andersin, R.A.; Ingram, D.S.; Zanier, A.M. Determining fracture pressure gradients from well logs. *J. Pet. Technol.* **1973**, *25*, 1259–1268. [CrossRef]
4. Aadnoy, B.S.; Belayneh, M. Elastic-plastic fracturing model for wellbore stability using non-penetrating fluids. *J. Pet. Sci. Eng.* **2004**, *45*, 179–192. [CrossRef]
5. Breckels, I.M.; Eekelen, H.A.M. Relationship Between Horizontal Stress and depth in sedimentary basins. *J. Pet. Sci. Eng.* **1982**, *34*, 2191–2199. [CrossRef]
6. Zhai, X.P.; Hao, H.Y.; Lou, Y.S.; Guan, H.X.; Ma, Z.L.; Lei, Y.C.; Zhang, H. Study on leakage pressure and its application in Halahatang sag. *Petrol. Geol. Recov. Eff.* **2013**, *20*, 108–110.
7. Zhai, X.P.; Chen, H.; Lou, Y.S.; Wu, H.M. Prediction and control model of shale induced fracture leakage pressure. *J. Pet. Sci. Eng.* **2020**, *198*, 108186. [CrossRef]
8. Majidi, R.; Miska, S.Z.; Yu, M.J.; Thompson, L.G.; Zhang, J. Modeling of drilling fluid losses in naturally fractured formations. In Proceedings of the SPE Annual Technical Conference and Exhibition, Denver, CO, USA, 21–24 September 2008; p. 114630. [CrossRef]
9. Chen, X.H.; Qiu, Z.S.; Yang, P.; Guo, B.Y.; Wang, B.T.; Wang, X.D. Dynamic simulation of fracture leakage process based on ABAQUS. *Drill. Fluid Complet. Fluid* **2019**, *36*, 15–19.
10. Laura, C.; Zoback, M.D.; Julio, F.; Vicki, S.; Chris, Z. Fracture characterization and fluid flow simulation with geomechanical constraints for a CO_2–EOR and sequestration project Teapot Dome Oil Field, Wyoming, USA. *Energy Procedia* **2011**, *4*, 3973–3980.
11. Majidi, R.; Miska, S.Z.; Thompson, L.G. Quantitative analysis of mud losses in naturally fractured reservoirs: The effect of rheology. *SPE Drill. Compl.* **2008**, *25*, 509–517. [CrossRef]
12. Peter, E.; Fan, Z.Q.; Julia, F.W. Geomechanical analysis of fluid injection and seismic fault slip for the Mw4.8 Timpson. Texas, earthquake sequence. *J. Geophys. Res. Solid Earth* **2016**, *121*, 2798–2812.
13. Ozdemirtas, M.; Kuru, E.; Babadagli, T. Experimental investigation of borehole ballooning due to flow of non-Newtonian fluids into fractured rocks. *Int. J. Rock Mech. Min. Sci.* **2010**, *47*, 1200–1206. [CrossRef]
14. Shahri, M.P.; Mehrabi, M. A new approach in modeling of fracture ballooning in naturally fractured reservoirs. In Proceedings of the SPE Kuwait International Petroleum Conference and Exhibition, Kuwait City, Kuwait, 10–12 December 2012; p. 163382. [CrossRef]
15. Zoback, M.D.; Apel, R. Upper crustal strength inferred from stress measurements to 6 km depth in the KTB borehole. *Nature* **1993**, *365*, 633–635. [CrossRef]

16. Panja, P.; Velasco, R.; Pathak, M.; Deo, M. Application of artificial intelligence to forecast hydrocarbon production from shales. *Petroleum* **2017**, *7*, 75–89. [CrossRef]

17. Ahmed, A.; Elkatatny, S.; Gamal, H.; Abdulraheem, A. Artificial intelligence models for real-time bulk density prediction of vertical complex lithology using the drilling parameters. *Arab. J. Sci. Eng.* **2022**, *47*, 10993–11006. [CrossRef]

18. Agin, F.; Khosravanian, R.; Karimifard, M. Application of adaptive neuro-fuzzy inference system and data mining approach to predict lost circulation using DOE technique (Case study: Maroon oilfield). *Petroleum* **2018**, *6*, 423–437. [CrossRef]

19. Alalimi, A.; Pan, L.; Al-Qaness, M.A.; Ewees, A.A.; Wang, X.; Abd Elaziz, M. Optimized Random Vector Functional Link network to predict oil production from Tahe oil field in China. *Oil Gas Sci. Technol. Rev. IFP Energ. Nouv.* **2021**, *76*, 3. [CrossRef]

20. Kim, J.; Park, J.; Shin, S.; Lee, Y.; Min, K.; Lee, S.; Kim, M. Prediction of engine NOx for virtual sensor using deep neural network and genetic algorithm. *Oil Gas Sci. Technol. Rev. IFP Energ. Nouv.* **2021**, *76*, 72. [CrossRef]

21. Guevara, J.; Zadrozny, B.; Buoro, A.; Lu, L.; Tolle, J.; Limbeck, J.W.; Hohl, D. A machine-learning methodology using domain knowledge constraints for well-data integration and well-production prediction. *SPE Reserv. Eval. Eng.* **2019**, *22*, 1185–1200. [CrossRef]

22. Abdulmalek, A.S.; Mahmoud, A.; Elkatatny, S.; Mahmoud, M.; Abdulazeez, A. Prediction of Pore and Fracture Pressures Using Support Vector Machine. In Proceedings of the International Petroleum Technology Conference, Beijing, China, 26–29 March 2019.

23. Li, Q.F.; Fu, J.H.; Peng, C.; Min, F.; Zhang, X.M.; Yang, Y.; Xu, Z.Y.; Bai, J.; Yu, Z.Q.; Wang, H. A deep learning approach for abnormal pore pressure prediction based on multivariate time series of kick. *Geoenergy Sci. Eng.* **2023**, *226*, 211715.

24. Yu, H.; Chen, G.X.; Gu, H.M. A machine learning methodology for multivariate pore-pressure prediction. *Comput. Geosci.* **2020**, *143*, 104548. [CrossRef]

25. Wang, J.; Cao, J.X.; Zhou, X. Reservoir porosity prediction based on deep bidirectional recurrent neural network. *Prog. Geophys.* **2022**, *37*, 267–274.

26. Yang, R.; Liu, X.; Yu, R.; Hu, Z.M.; Duan, X.G. Long short-term memory suggests a model for predicting shale gas pro-duction. *Appl. Energy* **2022**, *322*, 119415. [CrossRef]

27. Luo, F.Q.; Liu, J.T.; Chen, X.P. Intelligent method for predicting formation pore pressure in No. 5 fault zone in Shunbei oilfield based on BP and LSTM neural network. *Oil Drill. Prod. Technol.* **2022**, *44*, 506–514.

28. Peng, L.; Wang, L.; Xia, D.; Gao, Q.L. Effective energy consumption forecasting using empirical wavelet transform and long short-term memory. *Energy* **2022**, *238*, 121756. [CrossRef]

29. Lim, S.C.; Huh, J.H.; Hong, S.H.; Park, C.Y.; Kim, J.C. Solar Power Forecasting Using CNN-LSTM Hybrid Model. *Energies* **2022**, *15*, 8233. [CrossRef]

30. Zheng, D.; Ozbayoglu, E.; Miska, S.; Liu, Y. Cement Sheath Fatigue Failure Prediction by ANN-Based Model. In Proceedings of the Offshore Technology Conference, Houston, TX, USA, 2–5 May 2022.

31. Ehsan, B.; Ebrahim, B.D. Computational prediction of the drilling rate of penetration (ROP): A comparison of various machine learning approaches and traditional models. *J. Pet. Sci. Eng.* **2022**, *210*, 110033.

32. Wang, J.; Cao, J.; Yuan, S. Shear wave velocity prediction based on adaptive particle swarm optimization optimized re-current neural network. *J. Pet. Sci. Eng.* **2020**, *194*, 107466. [CrossRef]

33. Hochreiter, S.; Schmidhuber, J. Long short-term memory. *Neural Comput.* **1997**, *9*, 1735–1780. [CrossRef]

34. Zendehboudi, S.; Rezaei, N.; Lohi, A. Applications of hybrid models in chemical, petroleum, and energy systems: A systematic review. *Appl. Energy* **2018**, *228*, 2539–2566. [CrossRef]

35. Pan, S.; Wang, C.; Zhang, Y.; Cai, W. Lithologic identification based on long-term and short-term memory neural net-work to complete logging curve and hybrid optimization xgboost. *J. China Univ. Pet.* **2022**, *46*, 62–71.

36. Xu, K.; Shen, X.; Yao, T.; Tian, X.; Mei, T. Greedy layer-wise training of long-short term memory networks. In Proceedings of the 2018 IEEE International Conference on Multimedia & Expo Workshops (ICMEW), San Diego, CA, USA, 23–27 July 2018; pp. 1–6.

37. Ao, L.; Pang, H. Prediction of POR Based on Artificial Neural Network with Long and Short Memory (LSTM). In Proceedings of the 55th US Rock Mechanics/Geomechanics Symposium, Virtual, 18–25 June 2021; OnePetro: Richardson, TX, USA, 2021.

38. Abdollahi, H. A novel hybrid model for forecasting crude oil price based on time series decomposition. *Appl. Energy* **2020**, *267*, 115035. [CrossRef]

39. Chang, Z.; Zhang, Y.; Chen, W. Electricity price prediction based on hybrid model of adam optimized LSTM neural net-work and wavelet transform. *Energy* **2019**, *187*, 115804. [CrossRef]

40. Zheng, D.; Miska, S.; Ziaja, M.; Zhang, J. Study of anisotropic strength properties of shale. *AGH Drill. Oil Gas* **2019**, *36*, 93–112. [CrossRef]

41. Bajolvand, M.; Ramezanzadeh, A.; Mehrad, M.; Roohi, A. Optimization of controllable drilling parameters using a novel geomechanics-based workflow. *J. Pet. Sci. Eng.* **2022**, *218*, 111004. [CrossRef]

42. Kennedy, J.; Eberhart, R. Particle swarm optimization. In Proceedings of the ICNN'95-International Conference on Neural Networks, Perth, WA, Australia, 27 November–1 December 1995; pp. 1942–1948.

43. Huo, F.; Chen, Y.; Ren, W.; Dong, H.; Yu, T.; Zhang, J. Prediction of reservoir key parameters in 'sweet spot' on the basis of particle swarm optimization to TCN-LSTM network. *J. Pet. Sci. Eng.* **2022**, *214*, 110544. [CrossRef]

44. Zhou, C.; Gao, H.; Gao, G.; Zhang, W. Particle swarm optimization. *Comp. Appl. Res.* **2003**, *20*, 7–11.

45. Aguila-Leon, J.; Vargas-Salgado, C.; Chiñas-Palacios, C.; Díaz Bello, D. Energy management model for a standalone hy-brid microgrid through a particle Swarm optimization and artificial neural networks approach. *Energy Convers. Manag.* **2022**, *267*, 115920. [CrossRef]

46. Xue, L.; Gu, S.; Wang, J.; Liu, Y.; Tu, B. Prediction of gas well production performance based on particle swarm optimiza-tion and short-term memory neural network. *Petrol. Drill. Prod. Technol.* **2021**, *43*, 525–531.

47. Wang, X.; Deng, W.; Qi, W. Short term power load forecasting model based on hyper-parametric optimization. *Foreign Electron. Meas. Technol.* **2022**, *41*, 152–158.